Journal of Sol-Gel Science and Technology (2020) 95:562–572
https://doi.org/10.1007/s10971-020-05356-2

ORIGINAL PAPER: FUNCTIONAL COATINGS, THIN FILMS AND MEMBRANES (INCLUDING DEPOSITION TECHNIQUES)

Mechanisms for texture in $BaTiO_3$ thin films from aqueous chemical solution deposition

Kristine Bakken[1] · Anders Bank Blichfeld[1] · Dmitry Chernyshov[2] · Tor Grande[1] · Julia Glaum[1] · Mari-Ann Einarsrud[1]

Received: 22 January 2020 / Accepted: 26 June 2020 / Published online: 18 July 2020

Abstract

The prototype piezoelectric material $BaTiO_3$ is widely used in e.g., capacitators. Chemical solution deposition (CSD) of $BaTiO_3$ films is a simple and environmentally friendly processing route, but insight in the crystallization process is crucial to tailor the film properties. In this work, the influence of the annealing conditions on the crystallization behavior of $BaTiO_3$ thin films from *aqueous* chemical solution deposition is presented. In situ synchrotron X-ray diffraction was used to reveal the phase evolution, crystallization of the films, and to study how the degree of crystallographic texture in the polycrystalline films evolved. Our results revealed that the formation of an intermediate metastable oxycarbonate phase is critical for the formation of $BaTiO_3$ thin films prepared by aqueous CSD. The pyrolysis products present in the film before crystallization determine the degree of preferential orientation and by tuning the heating program, especially the heating rate through nucleation (<0.2 °C/s), control of the microstructure and degree of preferential orientation in the films was demonstrated.

Graphical Abstract

In situ X-ray diffraction patterns of a $BaTiO_3$ film, prepared by spin coating of an aqueous chemical solution, as a function of time and temperature, showing the phase evolution and crystallization of $BaTiO_3$.

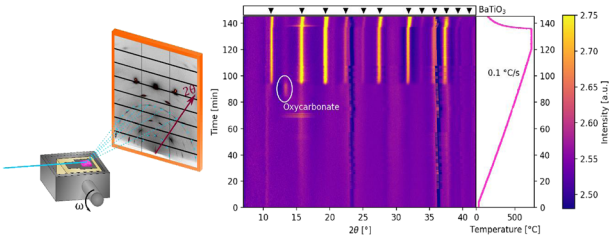

Keywords In situ X-ray diffraction · Texture · Barium titanate · Thin film · Chemical solution deposition

Supplementary information The online version of this article (https://doi.org/10.1007/s10971-020-05356-2) contains supplementary material, which is available to authorized users.

✉ Mari-Ann Einarsrud
mari-ann.einarsrud@ntnu.no

[1] Department of Materials Science and Engineering, NTNU Norwegian University of Science and Technology, Trondheim, Norway

[2] Swiss-Norwegian Beamlines, European Synchrotron Radiation Facility, Grenoble, France

Highlights

- In situ synchrotron X-ray diffraction revealed the phase evolution and crystallization of $BaTiO_3$ films prepared by aqueous CSD.
- An intermediate metastable oxycarbonate phase is critical for the formation of $BaTiO_3$ thin films.
- The pyrolysis process determines the degree of preferential orientation in the films.
- The microstructure and preferential orientation of the $BaTiO_3$ films can be tailored by the new insight.

1 Introduction

Piezo- and ferroelectric materials, such as $BaTiO_3$, are of general interest since they can convert mechanical energy into electricity and vice versa [1]. $BaTiO_3$ is widely used in e.g., capacitors due to the high dielectric constant, but ferroelectric materials are also applied as memory devices, sensors, actuators, and transducers [1]. For several of these applications the material is used as a thin film to enable miniaturization of the devices, but also to enhance the piezoelectric properties due to texturing of the films. Flexible energy harvesters, nanogenerators, and in vivo sensors are new possible applications where ferroelectric thin films are extremely attractive due to the ferroelectric properties, but also lowered operating voltage and fabrication more compatible with semiconductor technology [1, 2]. However, for these applications, deposition routes to high quality films with high degree of crystallographic texture need to be developed in order to fully utilize the potential of the materials.

CSD is a well-suited, inexpensive, and flexible method for fabrication of oxide thin films on an industrial scale [3, 4]. The synthesis is simple, as a stable precursor solution with the desired metal cations is deposited onto a substrate by e.g., spin coating before the film is annealed. Depending on the precursor solution chemistry and the heating profile used, different pyrolysis and crystallization reactions occur. Usually, a Rapid Thermal Processing unit (RTP) is used for annealing the films, as a high heating rate (20–50 °C/s) will avoid formation of unwanted secondary phases and achieve highly textured films [3, 4]. Lead-based ferroelectric films based on $Pb_{x-1}Zr_xTiO_3$ (PZT) are industrially produced by CSD, but synthesis routes for other dielectric and ferroelectric material classes have also been developed [3, 4]. $BaTiO_3$ thin films made by CSD are reported to have different microstructures, from polycrystalline films with columnar grains on platinized silicon (Pt/Si) [5–8] to distinct layers of small spherical grains on steel [9], copper foil [10], and Pt/Si [5–7, 11], but the microstructure is dependent on the precursor solution concentration [5–7]. Recently, Ræder et al. reported an aqueous-based synthesis route for $BaTiO_3$ thin films [12] where water-based precursor solutions make the fabrication process more environmental-friendly, and remove the need for toxic chemicals and inert atmospheres [3]. During this aqueous CSD process, the precursor developed into the crystalline perovskite phase through the formation of an intermediate metastable oxycarbonate phase [12]. This oxycarbonate phase with a proposed overall stoichiometry of $Ba_2Ti_2O_5CO_3$ [6, 13–21] is often observed in wet chemical synthesis of $BaTiO_3$, but local formation of a calcite-type modification of $BaCO_3$ ($R\bar{3}mH$, no. 166) is also reported [22, 23]. The oxycarbonate phase is reported to have diffuse reflections in X-ray diffraction (XRD) patterns, forming before or alongside the Bragg reflections of $BaTiO_3$, dependent on the annealing temperature [6, 18–24].

The report on epitaxial $BaTiO_3$ thin films on (100) $SrTiO_3$ (STO) [12] shows the potential to prepare films with a high degree of preferential orientation using CSD, but the mechanisms governing the crystallization was not fully investigated. In order to achieve tailored texture or epitaxy using CSD, it is necessary to understand how the processing parameters influence the pyrolysis reactions and the crystallization processes. The chemistry of the precursor solution plays an important role in CSD, as does the heating profile [3]. In this context, in situ XRD is a unique characterization method to investigate the mechanisms for nucleation and growth of crystalline phases during thermal annealing. The phase evolution and crystallization can be monitored directly during the decomposition, giving a thorough insight into the reactions taking place during the film annealing. By utilizing 2D detectors and the acquisition speed available, even the fast heating rates used in RTP's can be mimicked and this in situ methodology also allows a deeper investigation of the CSD process.

Here, we report on the conditions for achieving textured $BaTiO_3$ thin films on different substrates using aqueous CSD. Moreover, the factors that influence the microstructure of the film are also investigated. A novel in situ XRD characterization setup with high heating rates was used to reveal the processes taking place during the annealing and the crystallization patterns. The importance of understanding the ongoing reactions before and during crystallization is discussed in terms of choosing a suitable heating profile to obtain films with a given degree of texture and a designed microstructure. The pyrolysis step was found to be crucial for the degree of texture in the final film, while the microstructure is heavily dependent on the heating rate through nucleation.

Table 1 Summary of the synthesis and annealing conditions of the different films

Heating profile	Heating rate during crystallization	Annealing conditions	Substrate	Precursor concentration [M]
Multi-step (II)	25 °C/s	795 °C for 10 min	(100) STO	0.26
Multi-step (III)	25 °C/s	797 °C for 20 min	(100) STO	0.26
Multi-step (V)	25 °C/s	798 °C for 20 min	(100) STO	0.26
Multi-step (VI)	0.1 °C/s	796 °C for 30 min	(100) STO	0.26
Single-step (I)	25 °C/s	794 °C for 10 min	(100) STO	0.26
Single-step (IV)	0.03 °C/s	703 °C for 20 min	(100) STO	0.24
Single-step	0.1 °C/s	710 °C for 15 min	(100) STO	0.24
Single-step	0.2 °C/s	697 °C for 20 min	(100) STO	0.24
Single-step	1.57 °C/s	787 °C for 10 min	(100) STO	0.26
Single-step	0.2 °C/s	698 °C for 15 min	(110) STO	0.24
Single-step	0.2 °C/s	702 °C for 15 min	(111) STO	0.24
Single-step	2 °C/s	711 °C for 10 min	Pt/Si	0.24
Single-step	0.03 °C/s	695 °C for 30 min	Pt/Si	0.24

2 Experimental

The preparation of the aqueous precursor solution has been reported previously [12]. Separate Ba- and Ti-complex solutions were prepared and then mixed in stochiometric ratios to make two final $BaTiO_3$ precursor solutions with concentrations of 0.24 and 0.26 M. An EDTA-solution was prepared by dissolving EDTA (16.2 g, 98%, Sigma-Aldrich, St. Louis, MO, USA) in deionized water (75 mL) during heating to 60 °C under stirring and mixing with ammonia solution (34 mL, 30%, Sigma-Aldrich, St. Louis, MO, USA). $Ba(NO_3)_2$ (14.4 g, 99.9%, Sigma-Aldrich, St. Louis, MO, USA), dried at 200 °C for 12 h was added to the EDTA-solution, where citric acid (21.1 g, 99.5%, Sigma-Aldrich, St. Louis, MO, USA) was used as a secondary complexing agent. The solution was stirred until transparent before the pH was adjusted to neutral by addition of ammonia solution. The molar ratios were 1:1:5:2 for Ba $(NO_3)_2$, EDTA, ammonia, and citric acid, respectively. The Ti-solution was made by dissolving Ti-isopropoxide (17 mL, 97%, Sigma-Aldrich, St. Louis, MO, USA) in a citric acid solution (31.7 g citric acid in 75 mL water) at 80 °C in the molar ratio 1:3. The solution was kept at 80 °C with stirring for 12 h before the pH was adjusted to neutral by addition of ammonia solution. The concentration of Ti in the solution was determined by thermogravimetric analysis.

The films were deposited on (100), (110), and (111) single-crystal STO substrates (1×1 cm^2, Crystal-GMBH) and platinized silicon, $Pt/TiO_2/SiO_2/Si$ (Pt/Si) substrates (SINTEF, Oslo, Norway). Before film deposition, the substrates were rinsed in ethanol and subsequently plasma cleaned in oxygen atmosphere (Femto, Diener Electronic GmbH+Co, Ebhausen, Germany). A single layer of the precursor solution was deposited by spin coating at 3000 rpm for 30 s, followed by drying the films on a hotplate at 200 °C for 4 min in air, to prevent de-wetting of the film as the precursor solution does not form a gel after deposition. The resulting crystalline film thickness was 20–25 nm. An overview of the different samples and thermal processing conditions are presented in Table 1.

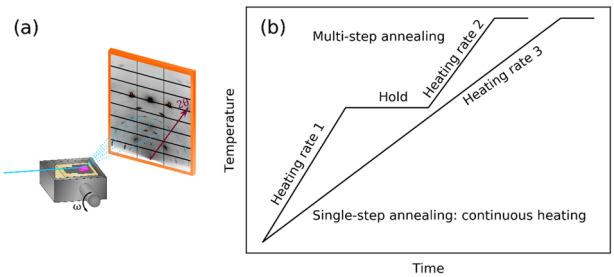

Fig. 1 **a** Illustration of the in-situ heating setup for thin film annealing relative to the X-ray beam and 2D-detector. **b** Schematics of the heating profiles used for annealing of the thin films during in situ synchrotron XRD measurements

Synchrotron XRD was conducted at the BM01 end-station, Swiss-Norwegian Beamlines (SNBL) at ESRF (The European Synchrotron Radiation Facility, Grenoble, France). The films were characterized at two different experimental sessions using wavelengths of 0.78449 Å and 0.77624 Å, which was chosen to suppress fluorescence from Sr in the STO substrates. A Pilatus2M 2D-detector was used [25], to be able to detect the azimuthal distribution of the diffracted intensity and to reveal the texture information. The films were heated in situ on a setup described in detail by Blichfeld et al. [26]. (shown in Fig. 1(a)) In short, a SiC heater (850 W, Bach Resistor Ceramics GmbH) was embedded in an insulating ceramic block. The films were placed on top of a Si wafer on the heater and held in place with a thermocouple, which also measured the film surface

temperature. A schematic of the different heating profiles used is presented in Fig. 1(b). Both heating and cooling of the films were conducted in air, and no cooling system was connected. The films were measured in grazing incidence to limit the signal from the substrate and they were aligned such that the beam footprint is centered in the film. For each dataset, the incident angle was rotated from 1° to 2° during data acquisition, so each detector frame was an average over this angle range to capture more reflections and compensate for any misalignments. To compensate for thermal expansion of the insulating ceramic block and SiC heater, the whole setup was shifted stepwise downwards with respect to the normal to the film, in order to keep the same position for the beam footprint during heating. The height steps and the exposure time was optimized for each experiment individually, based on the heating profile. A procedure for dealing with the thermal expansion and the height offset is described in Blichfeld et al. [26]. The signal from the substrate and thermal expansion data was combined to calculate the real sample to detect distance for each measurement height, and the data were corrected based on this calibration. The preliminary data processing and inspection of the powder diffraction profiles was done with BM01 software tools, such as BUBBLE [25] and MEDVED [27]. The final data processing was done in Jupyter Notebook utilizing the pyFAI package (see Blichfeld et al. [26]. for more details) accounting for corrections and calibrations specific for the given in situ setup. Rietveld refinement was done using MAUD software (Materials Analysis Using Diffraction v2.78) [28] to find the lattice parameter from the peak positions.

Scanning electron microscopy (SEM) of the thin films was performed using a field-emission FE-SEM Zeiss Ultra 55 LE microscope (Carl Zeiss AG, Oberkochen, Germany) with an in-lens detector. No coating was applied to the samples prior to imaging.

3 Results

3.1 Single-step annealing

The phase evolution and crystallization of a $BaTiO_3$ thin film on (100) STO during single-step annealing with a low heating rate (0.1 °C/s) is shown in Fig. 2. Before nucleation of $BaTiO_3$ at 570 °C, an intermediate oxycarbonate phase was present, seen from the diffuse diffraction line at $2\theta = 13.4°$ corresponding to the (012) reflection of the calcite-type $BaCO_3$ ($R\bar{3}mH$) [22, 23, 29]. This oxycarbonate phase has also been observed at intermediate temperatures when powders from the same precursor solutions were calcined at 550 °C [12]. The intensity of the reflection at $2\theta = 13.4°$ decreased at the expense of crystallization of $BaTiO_3$. The

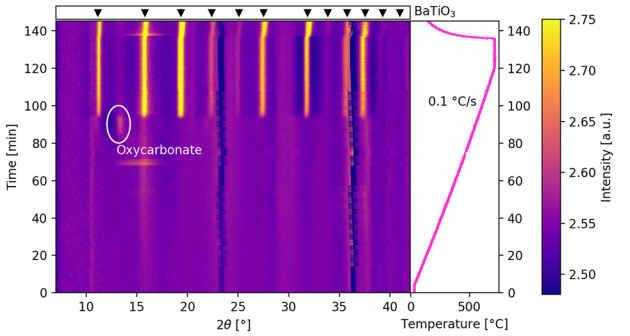

Fig. 2 Surface plot of in-situ diffractograms of a BaTiO3 thin film on (100) STO as a function of time with the corresponding temperature profile. The Intermediate oxycarbonate phase formed before the perovskite is indicated. The film was held at the maximum temperature of 710 °C for 15 min. Features at $2\theta = 10.3°$, 15.6°, 29.4°and 37.5° are due to diffuse scattering from the STO substrate. Any apparent features before the oxycarbonate are a result of the gaps in the detector, the data treatment, or diffuse scattering from the substrate

features at $2\theta = 10.3°$, 15.6°, 29.4° and 37.5° in Fig. 2 are due to diffuse scattering from the STO substrate. The apparent negative peaks at $2\theta = 23.0°$ and 36.1° are caused by gaps in the detector, which shift slightly in position from frame to frame.

Figure 3(a) shows a 2D diffractogram of the $BaTiO_3$ film, where the film texture is evident as there are district diffraction spots instead of full diffraction rings. The high degree of (100) preferred orientation is seen as the intense diffraction spot in the center of the (100) ring with hardly any distribution of this reflection along the diffraction ring. The (311) and (310) reflections from STO are also visible in the 2D diffractogram and the film diffraction spots are slightly beneath with limited intensity distribution on the diffraction ring, further demonstrating the high degree of (100) preferred orientation.

Cubic $BaTiO_3$ ($Pm\bar{3}m$, ICDD card #01-074-4539) was used in the Rietveld refinement and the calculated lattice parameter of $BaTiO_3$ at 710 °C was 4.0204(3) Å. The SEM image of the film displayed in Fig. 3(b) shows small spherical inter-necked grains ~50 nm in size, with an incomplete coverage of the STO substrate.

A summary of the crystallization behavior as a function of heating rate for single-step annealing of $BaTiO_3$ thin films on different substrates is presented in Fig. 4. For fast heating (>3 °C/s) no texture was observed and the oxycarbonate phases and perovskite nucleated simultaneously. For ultrafast heating (>10 °C/s), $BaTiO_3$ nucleated directly without any secondary or intermediate phases. These heating rates are in the range of what is commonly employed during RTP annealing of thin films. The maximum heating rate to obtain texture was ~3 °C/s, inferred from the increasing degree of texture observed at lower heating rates. In the case of the textured films, the oxycarbonate phase

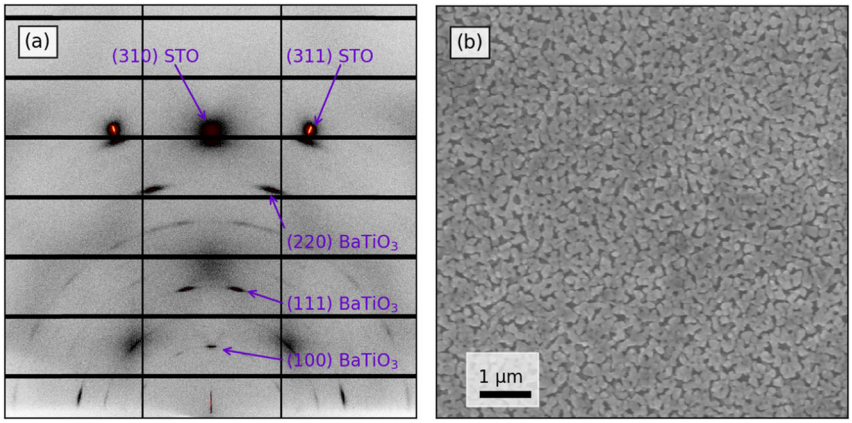

Fig. 3 **a** 2D diffractogram of a $BaTiO_3$ thin film on (100) STO after annealing at 710 °C for 15 min, heated with a heating rate of 0.1 °C/s showing the resulting film texture, and (**b**) SEM image of the microstructure of the film (top view)

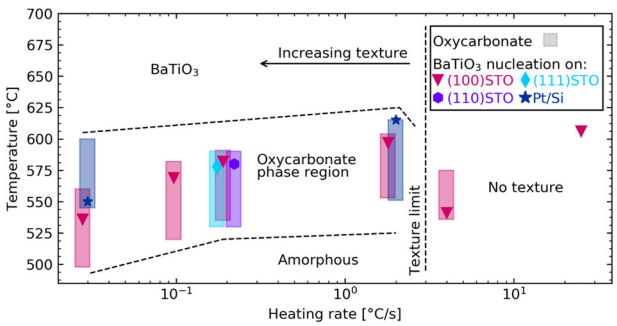

Fig. 4 Nucleation temperature (colored symbols) for BaTiO3 and temperature regions for presence of the intermediate oxycarbonate phase (colored rectangles) as a function of the heating rate used during in situ single-step annealing of BaTiO3 thin films. Stippled lines are guides for the eye

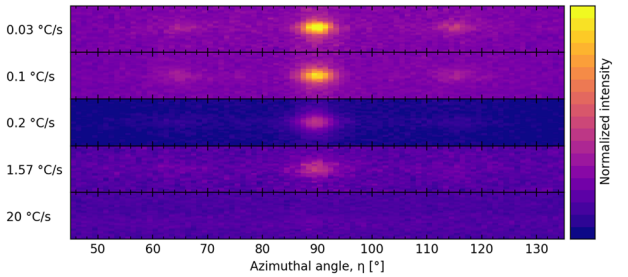

Fig. 5 Normalized azimuthal map for the (100) BaTiO3 diffraction for the films on (100) STO from single-step annealing showing the degree of (100) preferential orientation in the films. Diffractograms were recorded at ambient temperature after annealing

nucleated first, followed by nucleation of $BaTiO_3$, and the presence of the oxycarbonate phase normally remained for some time after the initial nucleation of $BaTiO_3$. The nucleation temperatures for both phases generally increased with increasing heating rate, and the temperature range for the presence of oxycarbonate (marked by colored rectangles) decreased with faster heating. The orientation of the STO substrates did not influence significantly the nucleation behavior. Deposition on Pt/Si stabilized the oxycarbonate phase over $BaTiO_3$, as can be seen from the broader temperature range for the oxycarbonate compared with the corresponding film on (100) STO.

The intensity and the azimuthal distribution of the (100) diffraction express the degree of preferential orientation in the films. The normalized azimuthal intensity of the (100) reflections along the diffraction ring for the films from single-step annealing on (100) STO are shown in Fig. 5. The film heated with a heating rate of 20 °C/s was polycrystalline, and the intensity of the (100) diffraction ring was so low that when normalized it is not visible in the azimuthal map (Fig. 5). The film heated with a heating rate of 1.57 °C/s had some degree of texture as well as full diffraction rings; the centered (100) reflection can be seen in the azimuthal map, while the full diffraction ring had too low an intensity after normalization. The intensity of the centered (100) reflection increases as a lower heating rate is used (Fig. 5), showing how the degree of preferential orientation increases as the heating rate decreases.

3.2 Multi-step annealing

Continuous heating with a fast rate (Film I in Fig. 6(a)), resulted in direct nucleation of the perovskite at a relatively high temperature. The resulting film was polycrystalline, which can be seen from the diffractogram in Fig. 6(c). The microstructure consists of small spherical grains with full film coverage (Fig. 6(d)). The nucleation behavior changed by introducing an intermediate dwell period at a certain temperature. If the hold step was in the temperature range for $BaTiO_3$ nucleation (Film II in Fig. 6(a)), the oxycarbonate formed before nucleation of $BaTiO_3$, and remained present until the temperature was increased due to the relative stability of the oxycarbonate in this temperature region. However, if the temperature during the hold step was significantly below the nucleation thresholds (Film III in Fig. 6(a)), the oxycarbonate phase was not formed, and the perovskite nucleated directly in the second heating period with the fast heating rate used throughout the

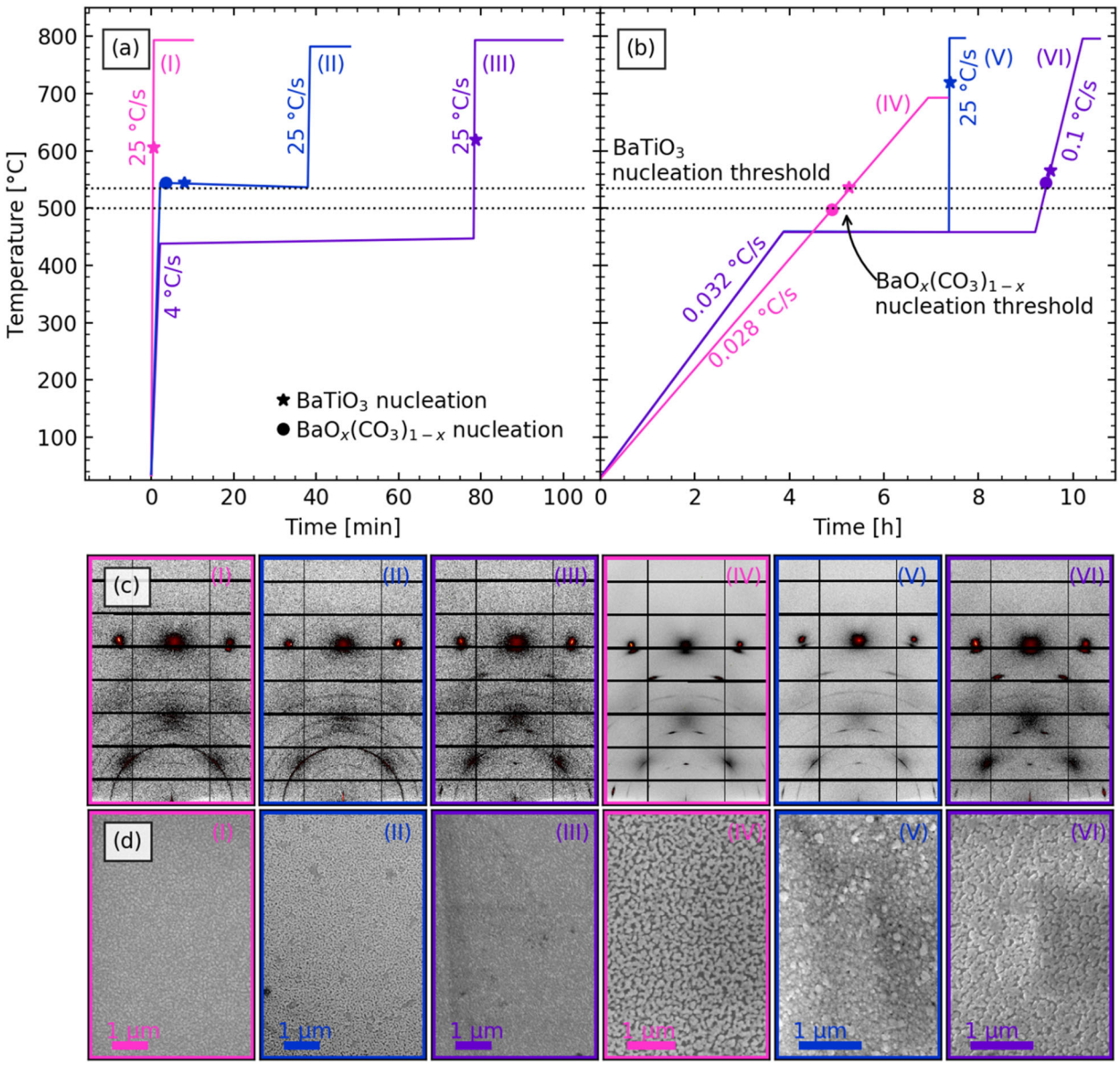

Fig. 6 Multi-step annealing heating program and nucleation temperatures of $BaTiO_3$ and oxycarbonate for (**a**) thin films with a short time below the nucleation thresholds and (**b**) long-time below the nucleation thresholds. (**c**) Diffractograms of the films with multi-step annealing after the being held at 800 °C for 10–30 min and (**d**) microstructure of the films after cooling (top view)

nucleation temperature region. Film III in Fig. 6(a) has some degree of texture, which can be seen from the 2D diffractogram in Fig. 6(c), even though a much higher heating rate was used than the texture limit observed for the single-step annealing to be about 3 °C/s. Hence, the time spent below the nucleation threshold temperature influences the degree of preferential orientation of the films. This is further illustrated by the films with a low heating rate before the hold step in Fig. 6(b), where all the films were highly textured (Fig. 6(c)), independent of the heating rate used during crystallization. Full coverage of the substrate and spherical grains of 15–20 nm are evident in the microstructure of the films with a high heating rate during nucleation (Film I, II, III, and V in Fig. 6(d)). For the films with low heating rate during nucleation (Film IV and VI), the coverage was incomplete, the grains were 45–60 nm in size and intergrown with some degree of necking between the different grains, resembling the microstructure of the single-step annealed film (Fig. 3(b)).

3.3 Rietveld refinements of in situ XRD patterns

Lattice parameter of $BaTiO_3$ determined by Rietveld refinements of the in situ XRD patterns of $BaTiO_3$ thin films on (100) STO for both single- and multi-step annealing are shown in Fig. 7. The data can be divided into two regimes.

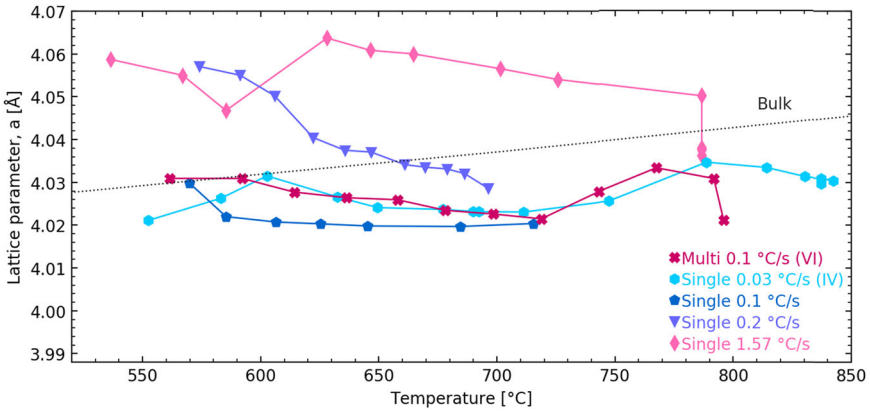

Fig. 7 Lattice parameters from Rietveld refinements as a function of temperature during both single-step and multi-step annealing of BaTiO3 thin films on (100) STO. Bulk values for the lattice parameter of $BaTiO_3$ based on thermal expansion data from Taylor [35] are included as the stippled line. Solid lines are guides to the eye

Table 2 Lattice parameters from Rietveld refinements of in situ diffractograms of $BaTiO_3$ thin film with different heating profiles on STO and Pt/Si substrates

Heating profile	Heating rate	Substrate	Lattice parameter [Å]	Texture
Multi-step (VI)	0.1 °C/s	(100) STO	4.0211(8) (792 °C)	Strong (100)
Single-step (IV)	0.03 °C/s	(100) STO	4.0298(6) (842 °C)	Strong (100)
Single-step	0.1 °C/s	(100) STO	4.0204(3) (710 °C)	Strong (100)
Single-step	0.2 °C/s	(100) STO	4.0256(6) (697 °C)	Strong (100)
Single-step	1.57 °C/s	(100) STO	4.0375(4) (787 °C)	Weak (100)
Single-step	20 °C/s	(100) STO	4.0502(1) (793 °C)	No texture
Single-step	0.2 °C/s	(110) STO	4.0276(9) (698 °C)	Strong (110)
Single-step	0.2 °C/s	(111) STO	4.0235(2) (702 °C)	Strong (111)
Single-step	2 °C/s	Pt/Si	3.9832(4) (711 °C)	No texture
Single-step	0.03 °C/s	Pt/Si	3.9775(8) (695 °C)	Yes

Values are from the last frame at high temperature. Crystallographic texture evaluated from the 2D diffractograms are also included

For the films with the lowest heating rates during nucleation (0.03 and 0.1 °C/s), $BaTiO_3$ nucleated with a lattice parameter close to the bulk value with no changes upon further heating. The films with a medium heating rate (0.2 and 1.57 °C/s) nucleated with a large lattice parameter relative to bulk $BaTiO_3$, which decreased upon further heating, converging toward a value below the bulk value in the same range as the films with lower heating rates. It should be noted that a direct comparison between the film and bulk lattice parameters is not straight-forward due to both finite size effects and strain in the films. All the films shown in Fig. 7 had some degree of texture and the microstructure is the same type as presented in Fig. 3(b) for the film with a heating rate of 0.1 °C/s, with necking between grains, incomplete coverage, and grains in the range 40–60 nm.

The lattice parameter from the Rietveld refinements and texture evaluated from the 2D diffractograms of $BaTiO_3$ thin films on STO and Pt/Si with different heating profiles are summarized in Table 2. For the films on (100) STO, the texture seen from the 2D diffractograms was the same for all films, shown in Fig. 3(a) for the single-step film with a heating rate of 0.1 °C/s. The intensity of the (100) diffraction spots on the 2D diffraction rings decreased for faster heating, demonstrating reduced texture with increased heating rate. The lattice parameter of the films on (100) STO were in general lower for films with a high degree of preferential orientation, showing that the texture influences the film crystal structure. The lattice parameters observed for films on (110) and (111) STO were comparable to the lattice parameters of the films on (100) STO (Table 2), but the preferential orientation followed the substrate orientation.

The films on Pt/Si had significantly lower lattice parameters than the films on STO (Table 2), which could be due to strain. Both films on Pt/Si were polycrystalline with full rings, but for the film with a heating rate of 0.03 °C/s there are $BaTiO_3$ diffraction spots on the diffraction rings, showing that there is a certain degree of preferred orientation for $BaTiO_3$ on Pt/Si.

4 Discussion

The present in situ setup for XRD of thin films from aqueous CSD is unique and was used to reveal the conditions required to control crystallization and texture of $BaTiO_3$

thin films through the heating profile and the type of substrate used. In order to achieve a high degree of preferential orientation of films from CSD, both the heating profile and pyrolysis reactions are important. A high heating rate generally delays the decomposition/combustion of organics and nucleation of the crystalline film to a higher temperature due to kinetics. At higher temperature the driving force for nucleation is lower, and heterogeneous nucleation at the substrate is more favorable [3]. Heterogeneous nucleation at the substrate surface is generally desired as it will increase the likelihood of preferential orientation of the film. In addition, rapid heating usually inhibits the formation of unwanted secondary phases and promotes densification of the crystalline film [3]. However, this is highly dependent on the transformation pathway, e.g., which phases form in the system, which is governed by the precursor chemistry and temperature profile. Intermediate phases can alter the nucleation into a nonclassical regime by acting as nucleation sites or templates for the crystalline film. Thus, the pyrolysis reactions influence the crystallization behavior and can also determine the crystalline film texture [3]. Fè et al. showed the importance of the transformation pathway by changing the pyrolysis temperature and precursor chemistry and as a result achieved different preferred orientation for PZT films on Pt/Si [30].

4.1 Mechanisms for texture

The degree of preferential orientation of the $BaTiO_3$ films on STO by aqueous CSD depends on the heating rate for the single-step annealed films. For the multi-step annealing it was shown in Fig. 6 that the total annealing time below the nucleation threshold of both oxycarbonate and $BaTiO_3$ determines if preferred orientation is developed, but the heating rate during crystallization is important as well. Films V and VI in Fig. 6(b) illustrate the effect of processing parameters on the crystallographic texture of the films in the non-classical nucleation regime. Film V has a certain degree of preferential orientation because it has been annealed for a long-time below the nucleation threshold, even though a high heating rate (25 °C/s) was used during crystallization. In contrast, Film VI, which has the same first heating rate and hold temperature (but is held for a longer time), has a very high degree of preferential orientation because a low heating rate was used during crystallization. This shows that the nature of pyrolysis products existing in the films before the oxycarbonate and $BaTiO_3$ nucleation to a large degree determines the degree of preferential orientation in the film. Meanwhile the heating rate during crystallization merely enhances the preferred orientation during the prolonged annealing. This argument also holds for the single-step annealing, as a lower heating rate also entail a longer time at intermediate temperatures. The (100) preferential orientation observed in the films on STO could be enhanced by an epitaxial layer at the interface with the STO substrate, which has been observed for thin films from aqueous CSD in the $K_{0.5}Na_{0.5}NbO_3$ (KNN) system on STO [31]. Ræder et al. has recently shown that epitaxial $BaTiO_3$ films can be produced by the same aqueous CSD route, notably at significantly higher temperatures [12].

4.2 Pyrolysis reactions and oxycarbonate formation

The intermediate oxycarbonate phase was observed to form before crystallization of $BaTiO_3$. The composition of the intermediate metastable carbonate-rich phase during wet chemical synthesis of $BaTiO_3$ is widely discussed and a macroscopic stoichiometry of $Ba_2Ti_2O_5CO_3$ is frequently suggested [6, 13–21]. However, Ischenko et al. [22, 23]. observed that the intermediate oxycarbonate phase was not homogeneous, and consisted of Ba- and Ti-rich regions, where there was no clear single crystallographic phase in the Ti-rich areas. The Ba-rich regions were found to have a structure close to the high temperature calcite-type modification of $BaCO_3$ ($R\bar{3}mH$, no. 166), and contained no titanium [22, 23]. Ischenko et al. suggested that the Ba-rich regions consisted of $BaO_x(CO_3)_{1-x}$, where there is a substitution of O^{2-} and CO_3^{2-}, and that this substitution stabilizes the calcite-type structure of $BaCO_3$ [22, 23]. The oxycarbonate phase is also observed in powders made from the same precursor solutions as the films in this work, where oxycarbonate in the powders forms below 550 °C and becomes unstable above 650 °C [12]. Since the oxycarbonate phase is also observed in the films, this means that the decomposition process and pyrolysis reactions do not change from powders to films, and the formation mechanisms for the oxycarbonate and $BaTiO_3$ are the same. However, the boundary for the phase region of the oxycarbonate in the films is lower in temperature than for the powders [12], due to the reduced size. The thermogravimetric profile of the corresponding powder (Fig. S1(a)) shows that the main mass loss occurs in a narrow temperature range around 500 °C, corresponding to the nucleation threshold found for the film. The oxycarbonate forms at temperatures as low as 500 °C and can persist up to 620 °C dependent on the heating rate and type of substrate. In light of the IR and XRD series on the corresponding powders [12], this sharp mass loss can be interpreted as the decomposition reaction proposed by Ischenko et al. [22].

$$\begin{aligned}(\mathrm{Ba,Ti})-\text{precursor complex} &\rightarrow (1-y)\mathrm{BaO}_x(\mathrm{CO}_3)_{1-x} \\ &+ \mathrm{Ba}_y\mathrm{TiO}_{2+y} \rightarrow \mathrm{BaTiO}_3.\end{aligned} \quad (1)$$

The use of Pt/Si substrates increases the stability of the oxycarbonate phase as it persists higher in temperature compared with the corresponding film on STO. The nucleation temperature of oxycarbonate on Pt/Si is higher than on STO and unaffected by the heating rate, so

nucleation occurs at temperatures similar to the powders from the same precursor solution [12], demonstrating that the oxycarbonate forms more easily on STO. The crystallization temperature for $BaTiO_3$ on Pt/Si is also generally higher compared with STO substrates. It follows that there are more favorable nucleation conditions for $BaTiO_3$ on STO. Considering the similar crystal structures, the nucleation temperature for $BaTiO_3$ should be lowered by heterogenous nucleation at the substrate interface. Since both $BaTiO_3$ and oxycarbonate nucleate more easily on STO the decomposition reaction (Eq. 1) should be accelerated on STO, which explains the reduced oxycarbonate stability on STO relative to Pt/Si seen in this work.

The phases present before the oxycarbonate and the $BaTiO_3$ nucleate result from the heating profile but most importantly are controlled by the precursor chemistry. Based on the reaction proposed by Ischenko et al. [22]. in Eq. 1, the formation of Ba-deficient Ba_yTiO_{2+y} clusters without any long-range order and possibly also their orientation with respect to the substrate are governing the resulting film texture and could also act as templates for the $BaTiO_3$ crystallization. As the intermediate phases are evenly dispersed in the film, so are the $BaTiO_3$ nucleation sites, resulting in homogeneous nucleation throughout the film, independent of the placement of the heating source. No increased degree of heterogenous nucleation at the substrate was observed for the films annealed with the in situ heating setup used in this work [26] compared with annealing with a conventional RTP unit [12], which supplies heat from the film surface. In the case of annealing of a single layer (20–25 nm), all the $BaTiO_3$ films became phase pure above 620 °C, independent of the presence of the oxycarbonate, but the formation of the intermediate phase could be detrimental if each layer is not fully crystallized for multilayered films. Khomyakova et al. [32]. reported that in aqueous CSD of multilayer $Ba_{0.85}Ca_{0.15}Zr_{0.1}Ti_{0.9}O_3$ (BCZT) films, the oxycarbonate formation leads to phase segregation and a secondary $CaZrTi_2O_7$ phase if each layer was not fully crystallized before deposition of the next. The same reaction mechanisms as presented in Khomyakova et al. [32]. studying BCZT films should hold for the $BaTiO_3$ films as the precursor chemistry is similar and the same complexing agents were used. Ba is depleted from the perovskite phase by local high CO_2 pressure from the oxycarbonate decomposition, leading to areas with Ba-deficient Ba_yTiO_{2+y} phases and $BaCO_3$ (aragonite type). Cation segregation due to formation of secondary phases and alkali volatility has also been observed in KNN thin films from CSD, with similar precursor chemistries [31, 33]. A thorough understanding and control over the decomposition reactions and the transformation pathway for the precursors are therefore of outmost importance for producing high quality multilayer thin films with high degree of texture from CSD.

The crystallization of $BaTiO_3$ on Pt/Si follows the same trend as on STO, where the preferred orientation is governed by the pyrolysis products. With a transformation pathway where the pyrolysis products act as templates for the $BaTiO_3$ nucleation, the nature of the precursor phases would govern the resulting preferred orientation in the crystalline film. The precursor chemistry and heating profile are important for preferential orientation in the films, both of which are different for the (100) oriented $BaTiO_3$ films reported in the literature [3, 34] and the aqueous precursor solution in this work, which most likely is the explanation for any difference in preferred orientations.

4.3 Grain size and lattice parameter

Finally, the film microstructure, grain size, and lattice parameter were shown to depend on the heating rate during crystallization. If a high heating rate is used, the films have small spherical grains, full coverage and a large lattice parameter, whereas a low heating rate gives larger interconnected grains with incomplete coverage and nucleation with a lattice parameter close to the bulk value. This shows that the grain size follows classical nucleation theory, even if the texture does not. Classical nucleation theory predicts many small grains for fast heating, when the nucleation rate is high, and the entire film should transform simultaneously [3]. In contrast, for a low heating rate the nucleation rate is lower, which results in fewer grains, but these are allowed to coarsen by the prolonged annealing time, resulting in a microstructure of grains with necking. The lattice parameters of the $BaTiO_3$ thin films provided in Fig. 7 deviates from the bulk values due to both finite size effects and strain. The strain in the films stems from both the lattice mismatch and the difference in thermal expansion coefficients with respect to the substrate. The lattice parameter of $BaTiO_3$ is larger than for STO and Pt, which results in compressive strain as $BaTiO_3$ has a larger thermal expansion coefficient than STO [35] and Pt [36]. The film thickness during crystallization is important, as it could impact the nucleation conditions and relaxation of the films. In this work, all the films were 20–25 nm thick for a single-crystalline layer, so relaxation can be expected, which can give nonuniform strain in the films and contribute to the observed lattice parameters and microstructure. The $BaTiO_3$ films on Pt/Si have a significantly lower lattice parameter than on STO, which could be due to strain and the preferential orientation. The lattice parameter for the films on STO with medium heating rates (0.2 and 1.57 °C/s) is large at the time of nucleation showing the finite size effects. However, in general the lattice parameters on both STO and Pt/Si decreased with prolonged annealing at high

temperature, independent of the heating rate, showing the influence of the substrate lattice mismatch and the resulting strain. The $BaTiO_3$ lattice parameters were generally the lowest, close to the substrate lattice parameter, for the most textured films, meaning that with increasing texture the film is also more strained. The stain could also be enhanced by the prolonged annealing time necessary to achieve the highly textured films. This is promising since strained and highly textured film are desired as they exhibit better ferroelectric properties [2].

5 Conclusion

$BaTiO_3$ thin films from aqueous CSD were characterized by a novel setup for in-situ XRD. The in-situ analysis revealed that in order to achieve high quality $BaTiO_3$ thin films with a high degree of preferential orientation, the films should be heated slowly, and preferably with a prolonged hold step below 500 °C. The pyrolysis products that form below 500 °C appear to determine if there is preferential orientation in the film, while a low heating rate during crystallization enhances the film texture. Moreover, compared with results on the related BCZT system, complete crystallization of each layer before deposition of more layers should be beneficial in order to avoid cation segregation and secondary phases. In general, the degree of preferential orientation in films from CSD depends on the heating profile and precursor chemistry, and it is important to have a proper understanding of the pyrolysis reactions and how these are influenced by the processing parameters. In situ studies are therefore crucial for characterizing the crystallization behavior uninterrupted and for understanding the complex mechanisms governing crystallization in CSD film fabrication, as utilized in this study, in order to prepare high quality films.

Acknowledgements Financial support from NTNU and The Research Council of Norway under the Toppforsk program to the project (No 250403) "From Aqueous Solutions to oxide Thin films and hierarchical Structures" (FASTS) is gratefully acknowledged. The Research Council of Norway is also acknowledged for the support to the Norwegian Micro- and Nano-Fabrication Facility, NorFab, project number 245963/F50. Finally, we acknowledge the SNX council for allocation of the beamtimes at the Swiss-Norwegian Beamline (SNBL) synchrotron facilities at the ESRF (The European Synchrotron Radiation Facility, Grenoble, France) and the SNBL beamline staff for their support during the experiments. Open Access funding provided by NTNU Norwegian University of Science and Technology (incl St. Olavs Hospital - Trondheim University Hospital).

Compliance with ethical standards

Conflict of interest The authors declare that they have no conflict of interest.

References

1. Rödel J, Jo W, Seifert KTP, Anton EM, Granzow T, Damjanovic D (2009) Perspective on the development of lead-free Piezoceramics. J Am Ceram Soc 92(6):1153–1177. https://doi.org/10.1111/j.1551-2916.2009.03061.x
2. Acosta M, Novak N, Rojas V, Patel S, Vaish R, Koruza J, Rossetti GA, Rödel J (2017) $BaTiO_3$-based piezoelectrics: fundamentals, current status, and perspectives. Appl Phys Rev 4(4). https://doi.org/10.1063/1.4990046
3. Schwartz RW, Schneller T, Waser R (2004) Chemical solution deposition of electronic oxide films. Comptes Rendus Chim 7(5):433–461. https://doi.org/10.1016/j.crci.2004.01.007
4. Bassiri-Gharb N, Bastani Y, Bernal A (2014) Chemical solution growth of ferroelectric oxide thin films and nanostructures. Chem Soc Rev 43(7):2125–2140. https://doi.org/10.1039/c3cs60250h
5. Halder S, Schneller T, Waser R (2005) Crystallization temperature limit of $(Ba,Sr)TiO_3$ thin films prepared by a non oxocarbonate phase forming CSD route. J Sol-Gel Sci Technol 33(3):299–306. https://doi.org/10.1007/s10971-005-6379-6
6. Hasenkox U, Hoffmann S, Waser R (1998) Influence of precursor chemistry on the formation of $MTiO_3$ (M = Ba, Sr) ceramic thin films. J Sol-Gel Sci Technol 12(2):67–79. https://doi.org/10.1023/a:1026480027046
7. Hoffmann S, Hasenkox U, Waser R, Jia CL, Urban K (1997) Chemical solution deposited $BaTiO_3$ and $SrTiO_3$ thin films with columnar microstructure. In: Schlom DG, Eom CB, Hawley ME, Foster CM, Speck JS (eds) Epitaxial Oxide Thin Films Iii, vol 474. 1997 MRS Spring Meeting, San Franscisco, USA. p 9–14
8. Stawski TM, Vijselaar WJC, Göbel OF, Veldhuis SA, Smith BF, Blank DHA, ten Elshof JE (2012) Influence of high temperature processing of sol-gel derived barium titanate thin films deposited on platinum and strontium ruthenate coated silicon wafers. Thin Solid Films 520(13):4394–4401. https://doi.org/10.1016/j.tsf.2012.02.029
9. Borderon C, Averty D, Seveno R, Gundel HW (2008) Preparation and characterization of barium strontium titanate thin films by chemical solution deposition. Ferroelectrics 362:1–7. https://doi.org/10.1080/00150190801996973
10. Ihlefeld JF, Borland WJ, Maria JP (2007) Enhanced dielectric and crystalline properties in ferroelectric barium titanate thin films. Adv Funct Mater 17(7):1199–1203. https://doi.org/10.1002/adfm.200601159
11. Chen XF, Lu WQ, Zhu WG, Lim SY, Akbar SA (2003) Structural and thermal analyses on phase evolution of sol-gel $(Ba,Sr)TiO_3$ thin films. Surf Coat Technol 167(2-3):203–206. https://doi.org/10.1016/s0257-8972(02)00897-6

12. Raeder TM, Bakken K, Glaum J, Einarsrud MA, Grande T (2018) Enhanced in-plane ferroelectricity in $BaTiO_3$ thin films fabricated by aqueous chemical solution deposition. Aip Adv 8(10). https://doi.org/10.1063/1.5059549
13. Arima M, Kakihana M, Nakamura Y, Yashima M, Yoshimura M (1996) Polymerized complex route to barium titanate powders using barium-titanium mixed-metal citric acid complex. J Am Ceram Soc 79(11):2847–2856. https://doi.org/10.1111/j.1151-2916.1996.tb08718.x
14. Fang TT, Tsay JD (2001) Effect of pH on the chemistry of the barium titanium citrate gel and its thermal decomposition behavior. J Am Ceram Soc 84(11):2475–2478. https://doi.org/10.1111/j.1151-2916.2001.tb01038.x
15. Hennings D, Mayr W (1978) Thermal-Decomposition Of (Ba,Ti) Citrates Into Barium-Titanate. J Solid State Chem 26(4):329–338. https://doi.org/10.1016/0022-4596(78)90167-6
16. Hoffmann S, Waser R (1999) Control of the morphology of CSD-prepared (Ba,Sr)TiO_3 thin films. J Eur Ceram Soc 19(6-7): 1339–1343. https://doi.org/10.1016/s0955-2219(98)00430-0
17. Chen SY, Wang HW, Huang LC (2003) Role of an intermediate phase (Ba,Sr)(2)$Ti_2O_5CO_3$ in doped ($Ba_{0.7}Sr_{0.3}$)TiO_3 thin films. Mater Chem Phys 77(3):632–638. https://doi.org/10.1016/s0254-0584(02)00009-3
18. Tsay JD, Fang TT, Gubiotti TA, Ying JY (1998) Evolution of the formation of barium titanate in the citrate process: the effect of the pH and the molar ratio of barium ion and citric acid. J Mater Sci 33(14):3721–3727. https://doi.org/10.1023/a:1004636219542
19. Durán P, Capel F, Gutierrez D, Tartaj J, Bañares MA, Moure C (2001) Metal citrate polymerized complex thermal decomposition leading to the synthesis of $BaTiO_3$: effects of the precursor structure on the BaTiO3 formation mechanism. J Mater Chem 11(7):1828–1836. https://doi.org/10.1039/b010172i
20. Durán P, Gutierrez D, Tartaj J, Bañares MA, Moure C (2002) On the formation of an oxycarbonate intermediate phase in the synthesis of $BaTiO_3$ from (Ba,Ti)-polymeric organic precursors. J Eur Ceram Soc 22(6):797–807. https://doi.org/10.1016/S0955-2219(01)00392-2
21. Gablenz S, Abicht HP, Pippel E, Lichtenberger O, Woltersdorf J (2000) New evidence for an oxycarbonate phase as an intermediate step in $BaTiO_3$ preparation. J Eur Ceram Soc 20(8): 1053–1060. https://doi.org/10.1016/S0955-2219(99)00242-3
22. Ischenko V, Pippel E, Köferstein R, Abicht HP, Woltersdorf J (2007) Barium titanate via thermal decomposition of Ba,Ti-precursor complexes: the nature of the intermediate phases. Solid State Sci 9(1):21–26. https://doi.org/10.1016/j.solidstatesciences.2006.09.004
23. Ischenko V, Woltersdorf J, Pippel E, Köferstein R, Abicht HP (2007) Formation of metastable calcite-type barium carbonate during low-temperature decomposition of (Ba,Ti)-precursor complexes. Solid State Sci 9(3-4):303–309. https://doi.org/10.1016/j.solidstatesciences.2007.02.003
24. Kumar S, Messing GL, White WB (1993) Metal-Organic Resin Derived Barium-Titanate Formation of Barium Titanium: 1, Oxycarbonate Intermediate. J Am Ceram Soc 76(3):617–624. https://doi.org/10.1111/j.1151-2916.1993.tb03650.x
25. Dyadkin V, Pattison P, Dmitriev V, Chernyshov D (2016) A new multipurpose diffractometer PILATUS@SNBL. J Synchrotron Radiat 23:825–829. https://doi.org/10.1107/s1600577516002411
26. Blichfeld AB, Bakken K, Chernyshov D, Glaum J, Grande T, Einarsrud M-A (2020) Experimental setup for high-temperature in situ studies of crystallization of thin films with atmosphere control. J Synchrotron Radiat (Submitted)
27. Chernyshov D, Dyadkin V, van Beek W, Urakawa A (2016) Frequency analysis for modulation-enhanced powder diffraction. Acta Crystallogr Sect A 72(4):500–506. https://doi.org/10.1107/S2053273316008378
28. Lutterotti L (2010) Total pattern fitting for the combined size–strain–stress–texture determination in thin film diffraction. Nucl Instrum Methods Phys Res Sect B: Beam Interact Mater Atoms 268 (3):334–340. https://doi.org/10.1016/j.nimb.2009.09.053
29. Antao SM, Hassan I (2007) $BaCO_3$: high-temperature crystal structures and the Pmcn→R3m phase transition at 811 °C. Phys Chem Miner 34(8):573–580. https://doi.org/10.1007/s00269-007-0172-8
30. Fè L, Norga GJ, Wouters DJ, Maes HE, Maes G (2001) Chemical structure evolution and orientation selection in sol-gel-prepared ferroelectric Pb(Zr,Ti)O_3 thin films. J Mater Res 16(9): 2499–2504. https://doi.org/10.1557/JMR.2001.0342
31. Pham K-N, Gaukås NH, Morozov M, Tybell T, Vullum PE, Grande T, Einarsrud M-A (2019) Epitaxial $K_{0.5}Na_{0.5}NbO_3$ thin films by aqueous chemical solution deposition. 6 (1):180989. https://doi.org/10.1098/rsos.180989
32. Khomyakova E, Wenner S, Bakken K, Grande T, Glaum J, Einarsrud M-A (2020) On the formation mechanism of BCZT thin films by aqueous chemical solution deposition. J Eur Ceram Soc, 2020, under revision.
33. Helth Gaukås N, Dale SM, Ræder TM, Toresen A, Holmestad R, Glaum J, Einarsrud M-A, Grande T (2019) Controlling phase purity and texture of $K_{0.5}Na_{0.5}NbO_3$ thin films by aqueous chemical solution deposition. Materials 12(13):2042. https://doi.org/10.3390/ma12132042
34. Waser R, Schneller T, Ehrhart P, Hoffmann-Eifert S (2001) Chemical deposition methods for ferroelectric thin films. Ferroelectrics 259(1–4):205–214. https://doi.org/10.1080/00150190108008740
35. Taylor D (1985) Thermal-expansion data 8 Complex Oxides, ABO3, Perovskites. Trans J Br Ceram Soc 84(6):181–188
36. Arblaster JW (2006) Crystallographic Properties of Platinum NEW METHODOLOGY AND ERRATUM. Platin Met Rev 50(3):118–119. https://doi.org/10.1595/147106706x129088